



**Environmental
Science**
Nano

Influence of nano-CuO and -TiO₂ on deposition and detachment of *Escherichia coli* in two model systems

Journal:	<i>Environmental Science: Nano</i>
Manuscript ID	EN-ART-07-2019-000857.R1
Article Type:	Paper

SCHOLARONE™
Manuscripts

1
2
3 Application of nanotechnologies as more cost-efficient and environmentally-friendly alternatives to
4 conventional pesticides and fertilizers has been increasingly explored and employed. In parallel, recent
5 foodborne illness outbreaks associated with romaine lettuce have drawn attention to risks that are
6 related to microbial contamination from environmental waters, irrigation, and washing processes. While
7 many nanomaterials have potential to enhance crop yields, understanding of their interactions and
8 impacts on the fate of foodborne pathogens in diverse environmental conditions is lacking. This work
9 employs two promising nanoparticles for pesticides and fertilizer formulations, nano-CuO and nano-
10 TiO₂, and demonstrates their effects on bacterial deposition and release, potentially impacting biofilm
11 formation in agricultural environments and foodborne illness risks.
12
13
14
15
16
17
18
19
20
21
22
23
24
25
26
27
28
29
30
31
32
33
34
35
36
37
38
39
40
41
42
43
44
45
46
47
48
49
50
51
52
53
54
55
56
57
58
59
60

1
2
3
4 Influence of nano-CuO and -TiO₂ on deposition and
5
6
7
8 detachment of *Escherichia coli* in two model
9
10
11
12 systems
13
14
15
16

17 *Holly M. Mayton^a, Daniel White^a, Ian M. Marcus^b, Sharon L. Walker^{a,b*}*
18
19

20 ^aDepartment of Chemical and Environmental Engineering, University of California, Riverside,
21
22 CA, USA
23
24

25 ^bDepartment of Civil, Architectural, and Environmental Engineering, Drexel University,
26
27 Philadelphia, PA, USA
28
29

30
31 ***Corresponding Author:** Email: slw384@drexel.edu
32
33
34
35
36
37
38
39
40
41
42
43
44
45
46
47
48
49
50
51
52
53
54
55
56
57
58
59
60

Abstract

Growing evidence suggests that agricultural water quality is closely tied to food safety risks. Therefore, the presence of nanoparticles in environmental waters due to utilization as pesticides and fertilizers may have unintended consequences, as the effects of their interactions with foodborne bacteria are not well understood. This investigation utilizes a 2D parallel-plate flow cell and a 3D saturated sand column to systematically examine changes in bacterial transport trends due to nano-bio interactions under dynamic flow conditions. Two *Escherichia coli* species, O157:H7 and 25922, exposed to nano-CuO (<50 nm) and nano-TiO₂ (<150 nm), were used to mimic agriculturally relevant conditions. In flow cell experiments, the presence of nano-CuO increased deposition and minimized release of pathogenic *E. coli* O157:H7 on a model spinach surface, while nano-TiO₂ had no significant effects ($p > 0.05$). Attachment and detachment – as quantified by mass transfer rate coefficients – of *E. coli* 25922 from the leaf surface were not impacted by the presence of nanoparticles. No breakthrough was observed in the column experiments, with the exception of nano-TiO₂ eluted in the presence of *E. coli* O157:H7. However, column dissection revealed higher proportions of suspended particles retained in the upper portion of the column when either nanoparticle was present. This provides further evidence that nanoparticles affect bacterial deposition and release, potentially promoting biofilm formation and foodborne illness risks.

1. Introduction

Within the United States and globally, a significant portion of foodborne illness outbreaks are related to microbial contamination of fruits and vegetables^{1,2}. This is often caused by irrigation and washing processes, where water potentially harbors harmful bacteria, leading to microbial cross contamination³⁻⁵. *Escherichia coli* (*E. coli*) O157:H7 is a pathogenic bacteria of particular interest due to two 2018 foodborne illness outbreaks associated with romaine lettuce, in which at least 112 people were hospitalized and 5 deaths were reported due to contamination that was found in irrigation water⁶. The fate of pathogens within produce irrigation, washing, and processing steps remains of interest for public health, as several recent studies have raised concerns about the efficacy of common rinsing and disinfection procedures⁷⁻⁹.

In parallel with modern food safety challenges, nanoparticles are increasingly common in agricultural waters and are being widely considered for application as pesticides and soil amendments in agricultural operations¹⁰⁻¹⁵. Fungicide formulations containing copper (I) oxide have been employed in the U.S. since the 1950s, and in recent years nanoscale copper oxide (CuO) has gained attention for its potential to serve as a more cost-efficient and environmentally-friendly pesticide^{16,17}. For example, Ayoub et al. (2018) demonstrated that nano-CuO could effectively control the viability of cotton leafworm¹⁸. Other agricultural applications of nano-CuO have included inhibition of pathogenic wheat isolates and control of fungal infections of tomato plants^{19,20}. Similarly, titanium dioxide (TiO₂) nanoparticles have demonstrated potential as pesticides and as plant growth supplements²¹⁻²⁵. For example, nano-TiO₂ has been shown to enhance the growth of spinach leaves, as well as improve seed germination and seedling growth for wheat and parsley^{21,22,24}. More recently, Mattiello and Marchiol (2017) demonstrated that

1
2
3 nano-TiO₂ can positively promote vegetative growth and enhance nutritional value of barley
4 grains when applied throughout the plant growth process²⁵.
5
6

7
8
9 Efficient use of these nanofertilizers and nanopesticides may increase crop yields and
10 provide complementary or replacement technologies for conventional chemical inputs, reducing
11 agricultural runoff and resulting environmental impacts^{13,15}. However, further research is needed
12 to improve our understanding of the variety of mechanisms in which nanomaterials suppress
13 disease and enhance plant growth, which can have unintended consequences. For example, many
14 nanoparticles, including CuO and TiO₂, have been shown to induce stress and affect quorum
15 sensing for microbes in environmentally relevant conditions, which can influence the cells'
16 likelihood of deposition and ability to form biofilms²⁶⁻²⁸. A review of several copper-based
17 nanomaterials described toxic effects on some strains of *E. coli* and other microbes at
18 concentrations as low as 4 ppm in aquatic environments²⁹. Interactions between nano-TiO₂ and
19 *E. coli* were studied previously in quartz sand column transport experiments, which found that
20 the presence of *E. coli* reduced deposition of industrial grade nano-TiO₂³⁰. However, few studies
21 have utilized and compared applicable nanoparticles in agriculturally relevant scenarios, which
22 include their interactions with non-targeted bacteria^{30, 31}.
23
24
25
26
27
28
29
30
31
32
33
34
35
36
37
38
39
40
41

42 The work presented herein contributes to the understanding of aqueous interactions and
43 transport of a specific foodborne pathogen (*E. coli* O157:H7) and metal oxide nanoparticles,
44 specifically nano-CuO and nano-TiO₂ in agricultural systems. Non-pathogenic *E. coli* 25922,
45 which is a quality control strain commonly employed by the agricultural industry, is also used for
46 comparison to the pathogen in this study. A 2D parallel-plate flow cell and 3D saturated sand
47 column were used to systematically examine changes in bacteria deposition (also referred to as
48 attachment) and detachment trends as a result of nano-bio interactions under dynamic flow
49
50
51
52
53
54
55
56
57
58
59
60

1
2
3 conditions on model leaf and mineral surfaces. By studying these idealized systems in tandem,
4
5 the results provide unique insights into how physiochemical parameters of colloids affect their
6
7 interactions with more complex real-life environments^{30, 32}.
8
9

10 11 12 13 **2 Materials & Methods**

14 15 **2.1 Nanoparticle selection.**

16
17 Copper oxide (CuO) was selected as a model nanoparticle for this study because of its
18
19 use in agriculture as an herbicide¹⁸⁻²⁰. Nano-CuO was purchased from Sigma Aldrich (St. Louis,
20
21 MO) and was reported to have a primary particle size of <50 nm. This is similar to recent work
22
23 that has demonstrated agricultural applications of nano-CuO in the range of 40-60 nm^{19, 20}. Food
24
25 grade (FG) TiO₂ (anatase, E171, Arizona State University) was selected as the other model
26
27 nanoparticle with a primary particle size of 122 ± 48 nm, as measured by electron microscopy in
28
29 Yang *et al.* (2014)³³. These particles are significantly larger than the nano-TiO₂ that has been
30
31 used in some recent studies and commercial products (ranging from 10 to 60 nm)^{34, 35}. However,
32
33 these particles were chosen to minimize physiological impact to bacterial cells, while
34
35 maintaining application relevance of FG TiO₂, which has shown promise as a fungicide and a
36
37 plant growth enhancer^{34, 35}. On account of the photocatalytic activity of nano-TiO₂, all
38
39 suspensions were kept wrapped in foil to minimize UV light exposure during preparation. Both
40
41 nanoparticles were used at a concentration of 10 mg/mL, corresponding to 10⁹ and at least 10¹⁰
42
43 primary particles/mL for TiO₂ and CuO, respectively. The reported ranges of concentrations of
44
45 nanoparticle formulations for agricultural applications are from 0.005 – 50 mg/mL for TiO₂^{34, 35}
46
47 and 0.01 – 10 mg/mL for CuO¹⁸⁻²⁵. Therefore, a nanoparticle concentration of 10 mg/mL was
48
49 chosen, within the aforementioned environmentally relevant range, to maximize observable
50
51
52
53
54
55
56
57
58
59
60

1
2
3 effects while remaining below previously observed toxic concentrations of nano-TiO₂ and nano-
4
5 CuO^{37, 38}.
6
7
8
9

10 11 **2.2 Bacteria selection.**

12
13 *E. coli* O157:H7 and 25922 (ATCC 43888 and 25922) were chosen as model bacteria for
14 this study to represent a pathogenic and non-pathogenic strain, respectively. The strains were
15 acquired from the USDA (USDA-ERS-FAESR, Bowling Green, KY). *E. coli* O157:H7 has been
16 recently implicated in several major foodborne illness outbreaks associated with leafy greens⁴⁰,
17 while *E. coli* 25922 is a commonly used surrogate for assessing efficacy of food safety processes
18 in the agricultural industry⁴¹. *E. coli* cells were cultured overnight in Luria-Bertani (LB) broth
19 (Fisher Scientific, Fair Lawn, NJ) at 37 °C. The overnight culture was then diluted 1:100 in fresh
20 LB, incubated at 37 °C for 3.5 hours, and harvested at the mid-exponential cell growth phase by
21 washing and resuspending cells in 10 mM KCl⁴². For all experiments with each of the two
22 strains, scenarios tested were either suspensions of cells only, cells with CuO, or cells with TiO₂.
23
24
25
26
27
28
29
30
31
32
33
34
35
36
37
38

39 **2.3 Sample preparation and characterization.**

40
41 Stock nanoparticle solutions were prepared using dry nanoparticle powder and sonicated
42 for 30 min in 10 mM KCl. Then the pH of the solution was adjusted to 7.0 using KOH and HCl,
43 followed by 30 sec of sonication³⁶. For experiments with *E. coli*, concentrated bacteria stock was
44 then diluted in 10 mM KCl to an OD₆₀₀ of 0.2 (or 10⁹ cells/mL). Then, with or without bacteria,
45 nanoparticle solutions were gently shaken for 40 min to allow aggregation to occur and stabilize.
46 Mixed nanoparticle-bacteria samples were then used for either transport experiments or
47 physiochemical characterization within 2 hours of preparation.
48
49
50
51
52
53
54
55
56
57
58
59
60

1
2
3 Zeta potential and hydrodynamic diameter were determined for each suspension (10^9
4 cells/mL *E. coli*, 10 mg/mL nanoparticles, or a mixture) using a ZetaPALS analyzer and dynamic
5 light scattering (DLS), respectively (Brookhaven Instruments Corp., Holtsville, NY)³⁹.
6
7
8
9
10
11
12

13 **2.4 Parallel-plate experiments.**

14
15 In a parallel plate flow cell (GlycoTech, Rockville, MA), deposition and release of the
16 model *E. coli* on a spinach leaf surface was directly observed using an inverted microscope (BX-
17 52, Olympus) and digital camera (Demo Retiga EXI Monochrome, QImaging) as previously
18 described^{7, 43, 44}. All baby spinach leaves used in this study were pre-washed, bagged spinach
19 from the same brand and purchased from the same local grocery store. As detailed in Mayton *et*
20 *al.* (2019), epicuticle films were isolated from the spinach leaf surface through a freeze
21 embedding technique and transferred to a polycarbonate substrate, which were stored at 4 °C for
22 up to one week before use in the parallel-plate flow cell⁴⁵.
23
24
25
26
27
28
29
30
31
32
33
34

35 Cell suspensions were allowed to attach to the leaf surface at a flow rate of 0.1 mL/min
36 using a syringe pump over 30 min. This flow rate creates non-turbulent flow conditions and
37 simulates expected conditions in a gentle produce washing process or rain event⁴⁶. After a 5 min
38 rinse with sterile 10 mM KCl to remove reversibly attached cells, deionized (DI) water was
39 injected into the flow cell for 25 min to observe detachment. Over the course of the 60 min
40 experiment, photos were taken every 30 sec and a code developed using Matlab (Mathworks,
41 Natwick, MA) was used to quantify the number of cells attached or detached from the surface
42 over time. Enumeration of cells was then used to calculate attachment and detachment mass
43 transfer rate coefficients (k_{att} and k_{det} , respectively) as a function of bacteria flux (J , cells $\text{s}^{-1} \text{m}^{-2}$)
44 and concentration of cells in suspension (C_0 , cells/mL), where
45
46
47
48
49
50
51
52
53
54
55
56
57
58
59
60

$$k = \frac{J}{C_0}$$

Detachment is also reported as a percentage of cells removed based on the number of counted cells in the last frame of the attachment phase. Additionally, the duration of detachment (before the slope of cells vs. time reaches zero) varied and is therefore also presented in this study. Experimental scenarios with each combination of bacteria and nanoparticle, as well as each individual bacteria strain, were conducted in triplicate and statistical analysis was performed using a statistical single-factor ANOVA test for confidence intervals of 95% and 99% ($p < 0.05$ and $p < 0.01$, respectively).

2.5 Saturated sand column experiments.

In the 3D transport experiments through a quartz packed bed, the movement of *E. coli* and metal oxide nanoparticles in saturated soil conditions was observed using an in-line UV-VIS detector, as previously described^{47, 48} and documented in the supplementary information (SI). Briefly, the packed columns were primed with 10 mM KCl, before the aforementioned suspensions were pumped into the column at 2 mL/min for approximately 7.5 pore volumes (PV), followed by approximately 7.5 PV of 10 mM KCl, and 5 PV of DI water. This flow rate was chosen to mimic slow sand grain filtration and trickle flows through soil³¹. The column effluent flowed through a UV-VIS detector (TURNER SP-890) with an in-line cuvette. Absorbance measurements were taken every 30 sec at a wavelength of 600 nm to monitor the presence of nanoparticles and bacteria, and to generate breakthrough curves (see SI for further information). Scenarios included *E. coli* O157:H7 alone, with CuO, and with TiO₂, and were each conducted in triplicate. One control was conducted with *E. coli* 25922 in the absence of nanoparticles as a control experiment.

1
2
3 Column dissections were performed once for each experimental scenario to elucidate
4 differences in retention that may not be apparent from breakthrough curves⁴⁹. Using a modified
5 method from Lanphere *et al.* (2013) to minimize disruption of bacterial cells, sand was removed
6 from the column in one centimeter increments⁴⁹. The optical density (OD) of the supernatant
7 extracted from each sand segment was measured at 600 nm and normalized based on the weight
8 of the sand in the tube and the proportion to the total absorbance of all five, 1 cm sections.
9
10
11
12
13
14
15
16
17
18

19 **2.6 Scanning electron microscopy.**

20
21 Scanning electron microscopy (SEM) was utilized to visualize each bacterium and their
22 interactions with nanoparticle suspensions in order to corroborate and provide further insight into
23 the size distribution measured using dynamic light scattering described in Section 2.1. A MIRA3
24 GMU field emission SEM (TESCAN, Brno, Czech Republic) was used to acquire at least 5
25 images of suspensions from each experimental condition (cells only or cells plus nanoparticles).
26 For imaging by SEM, 15 μL of each sample (10 \times diluted to 1 mM KCl) was dispensed and dried
27 onto polycarbonate coupons, sputter coated with gold/palladium, and analyzed at 15 kV
28 accelerating voltage, using low vacuum mode at a working distance of 4.80 mm.
29
30
31
32
33
34
35
36
37
38
39
40
41

42 **3 Results & Discussion**

43 **3.1 Critical observations and implications for pathogen fate.**

44
45 The results gleaned from this study provide insight into deposition and detachment trends
46 of agriculturally relevant bacteria and nanomaterial mixtures by using fundamental 2D and 3D
47 transport models. The 2D model spinach environment (parallel plate flow cell) provided a
48 physically simple, but chemically heterogeneous, environment for direct observation of cell
49
50
51
52
53
54
55
56
57
58
59
60

1
2
3 attachment and detachment. Meanwhile, the 3D packed bed provided a physically complex, but
4
5 chemically simple environment where cell deposition and detachment were indirectly observed.
6
7 Both systems involved negatively charged collector surfaces, but the hydrodynamics of the two
8
9 systems have been demonstrated to foster different modes of colloidal deposition⁴⁰. However, the
10
11 particle Peclet numbers in the column and parallel plate chamber are comparable, and are
12
13 expected to be within the diffusion-limited regime^{39, 47}. Together, the 2D and 3D systems provide
14
15 corroborating evidence of the role of irreversible attachment in bacterial fate and transport in the
16
17 simulated agriculturally relevant scenarios.
18
19
20
21

22
23 In the results presented below, the presence of 10 mg/mL of nanoparticle food grade TiO₂
24
25 particles during bacterial deposition resulted in a steady or slightly increased release of
26
27 pathogenic *E. coli* O157:H7 from leaf and sand surfaces during a gentle rinse afterwards. This
28
29 suggests that the application of TiO₂ may promote reversible bacterial attachment and presents a
30
31 safety consideration due to bacteria release, which can allow for more efficient decontamination
32
33 of planktonic cells or can cause cross contamination during a food rinsing process or rain event.
34
35 The presence of nano-CuO lead to an increase in bacterial attachment and decrease in
36
37 detachment on both leaf and sand surfaces, possibly fostering increased food illness risk by
38
39 enhancing irreversible attachment, a critical early stages of the biofilm formation process^{50, 51}.
40
41
42

43
44 The effects of these nanoparticles were observed to be more pronounced on the transport
45
46 of *E. coli* O157:H7 than the common non-pathogenic quality control strain, *E. coli* 25922, as
47
48 transport of the more neutrally charged pathogen may be more sensitive to changes in the
49
50 suspension fluid. This may lead to underestimation of changes in microbial risks through the
51
52 food system as a result of using nanomaterials in agricultural operations. Also of environmental
53
54 relevance is the observed decrease in deposition of TiO₂ in clean bed filtration in the presence of
55
56
57
58
59
60

1
2
3 bacteria. This may be due to increased stability associated with extracellular polymeric
4 substances (EPS) on the nanoparticle surface, and may lead to enhanced transport of TiO₂ in
5 soils. The influence of nano-bio interactions on bacterial transport in agricultural scenarios
6 varied by cell type and nanoparticle type: copper oxide nanoparticles increased irreversible
7 pathogen attachment, while titanium dioxide nanoparticles slightly increased pathogen transport.
8
9 The results of this work contribute to greater understanding of the associated food safety and
10 environmental risks.
11
12
13
14
15
16
17
18
19
20

21 **3.2 Nanoparticle and bacteria characterization.**

22 *3.2.1 Physicochemical characterization.*

23
24
25
26 The electrophoretic mobility and average effective diameter of suspensions comprised of
27 each type of nanoparticles, *E. coli*, and the relevant mixtures are displayed in Table 1. At pH 7,
28 CuO is near its isoelectric point and therefore - under the solution chemistry conditions of this
29 study - the particles are close to neutrally charged (-6.11 ± 3.6 mV)⁵². TiO₂ is far from its
30 isoelectric point and therefore is more negatively charged at the test pH of 7 in these suspensions
31 (-34.5 ± 9.6 mV)⁵³. Due to the greater magnitude of charge of TiO₂, these particles are more
32 repulsive and therefore form smaller aggregates relative to their primary particle size (758 ± 111
33 relative to approximately 120 nm) than CuO (468 ± 28 relative to <50 nm). For the nanoparticles
34 alone, the calculated zeta potential and effective diameter are similar to those of previous work
35 with these metal oxide particles⁵²⁻⁵⁴.
36
37
38
39
40
41
42
43
44
45
46
47
48
49

50 In agreement with previous studies, both bacteria cells are negatively charged in these
51 conditions, with *E. coli* 25922 highly negatively charged (-44.4 ± 2.1), while *E. coli* O157:H7 is
52 close to neutral (-3.4 ± 0.3)^{41, 55}. Comparing the hydrodynamic diameters, *E. coli* 25922 cells are
53
54
55
56
57
58
59
60

1821 ± 125 nm while *E. coli* O157:H7 cells are smaller at 1410 ± 161 nm. With the addition of 10 mg/mL of each nanoparticle, the relative proportion of bacterial cells to nanoparticles (in numbers) was on the order of 1:1 for nano-TiO₂ and 1:10 for nano-CuO. Additional information on the calculation of bacteria:nanoparticle ratios is available in Table S1. The net charge of the particles in suspension, as measured by zeta potential, was not significantly affected with CuO in suspension ($p > 0.05$), but measurements showed significantly more negatively charged colloids with TiO₂ present ($p < 0.01$). The measured effective hydrodynamic diameter of the suspensions was apparently reduced by the presence of nanoparticles, compared to the bacteria alone. Due to limitations in of using dynamic light scattering to assess particle size in mixed-particle systems, results for suspension of bacteria and nanoparticles together are most useful for the observation of trends, rather than absolute values. Further discussion is provided in the Supporting Information.

Table 1. Characterization of each bacteria, nanoparticle, and combination.

Bacteria	Nanoparticle	Effective diameter (nm) ^a	Zeta potential (mV) ^b
<i>E. coli</i> O157:H7	--	1410 ± 161	-3.4 ± 0.3
<i>E. coli</i> O157:H7	CuO	1221 ± 155	-4.0 ± 0.6
<i>E. coli</i> O157:H7	TiO ₂	608 ± 71	-10.0 ± 0.4
<i>E. coli</i> 29522	--	1821 ± 125	-44.4 ± 2.1
<i>E. coli</i> 29522	CuO	1327 ± 38	-44.9 ± 1.2
<i>E. coli</i> 29522	TiO ₂	1209 ± 205	-45.1 ± 1.1
--	CuO	468 ± 28	-6.1 ± 3.6
--	TiO ₂	758 ± 111	-34.5 ± 9.2

^a Measured using dynamic light scattering (DLS)

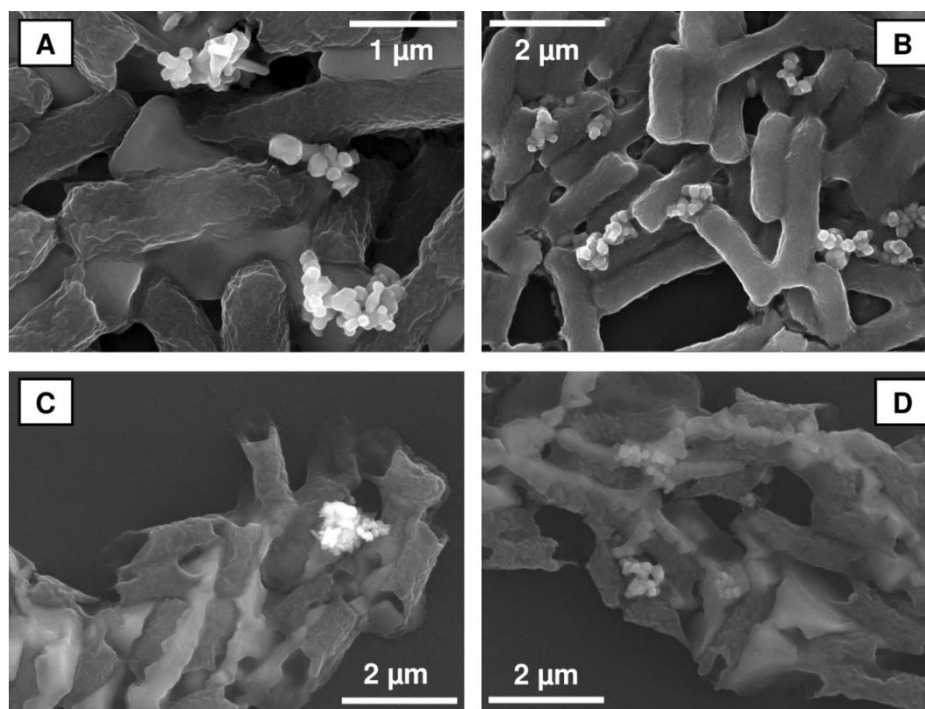
^b Measured using ZetaPALS via electrophoretic mobility

*Standard deviation calculated from triplicate experiments

3.2.2 SEM images.

To corroborate size and surface charge results, SEM images were taken of the bacteria and nanoparticle mixtures (Figure 1). Overall, nanoparticles are well-incorporated in bacteria

1
2
3 aggregates for both strains of *E. coli*. Nanoparticle aggregation up to approximately 1 μm
4 diameter aggregates is evident in these conditions for both CuO and TiO₂. This result is slightly
5 larger than what is expected based on dynamic light scattering results in Table 1, as well as
6 larger than what is expected based on dynamic light scattering results in Table 1, as well as
7 previous work with these nanoparticles in low ionic strength and pH 7 solutions^{29,30}. For *E. coli*
8 O157:H7, images show well-defined cells and nanoparticle aggregates. In contrast, obtaining
9 sharp and clear photos of nanoparticle aggregates in the *E. coli* 25922 mixture was more difficult
10 since 25922 has visibly more EPS than O157:H7, prepared at the same conditions (Figure 1).
11 These images provide evidence that EPS can cover some portion of the nanoparticle surface in
12
13
14
15
16
17
18
19
20
21
22



45 suspension.

46
47
48 **Figure 1. SEM images of *E. coli* O157:H7 (A, B) and *E. coli* 25922 (C, D).** Images were captured after
49 suspensions with 10 mg/mL of either CuO (A, C) or TiO₂ (B, D) in 10 mM KCl were deposited and dried on
50 polycarbonate coupons using a modified version of the methods previously described by Chowdhury et al. (2012)³⁰.

51 **3.2.3 DLVO predictions.**

1
2
3 Given that the maximum ratio of bacteria cells to nanoparticles was 1:20, it is not
4 surprising to see that most bacteria are not coated in nanoparticles. However, SEM images show
5 interactions in which nanoparticles are often positioned tightly between two or more bacteria.
6
7 This is notable because physical interactions have been shown to be one of the primary
8 mechanisms by which nanoparticles induce stress in bacteria cells^{18, 56, 57}. For example, previous
9 work with antibacterial silver nanoparticles found that electrostatic forces were a primary
10 mechanism of nanoparticle adsorption to bacteria surfaces⁵⁸. Studies with both nano-CuO and -
11 TiO₂ have documented the importance of proximity to the cell surface to induce the toxic effects
12 of copper ions and reactive oxygen species on gram positive and gram negative bacteria⁵⁷.
13
14
15
16
17
18
19
20
21
22
23
24

25 Colloidal size and surface charge results were used to predict the electrostatic and van der
26 Waals forces between particles and cells, and between heteroaggregates and collector surfaces,
27 using Derjaguin-Landau-Verwey-Overbeek (DLVO) theory⁵⁹. Traditional electrokinetic
28 characterization and application of DLVO theory provides insight into the interactions between
29 cells and nanoparticles, as well as with the plant and mineral surfaces. Non-pathogenic *E. coli*
30 25922 cells had a greater magnitude of measured zeta potential than the pathogenic strain
31 (O157:H7) (-44.4 ± 2.1 and -3.4 ± 0.3 mV, respectively), which resulted in greater predicted
32 repulsive forces between cells and other negatively charged surfaces, such as the nanoparticle,
33 leaf, and quartz sand surfaces. Therefore, it was anticipated that the non-pathogen cells would be
34 more stable in the environment than the pathogen, which was expected to result in greater
35 interactions between the leaf or sand substrates, and therefore less mobile. With addition of
36 nanoparticles in suspension that may associate with the bacteria surface, the overall effective
37 shape of a cell with a nanoparticle adhered to its surface was considered unchanged. Using this
38 assumption, one would not expect to observe significant differences in bacterial transport with
39
40
41
42
43
44
45
46
47
48
49
50
51
52
53
54
55
56
57
58
59
60

1
2
3 the addition of nanoparticles based on DLVO. However, significant impacts are observed in 2D
4 and 3D transport scenarios, suggesting that other mechanisms may be involved. Additionally, the
5 potential formation of irregularly shaped bacteria-nanoparticle aggregates and their interactions
6 with the leaf and grain surfaces presents a challenge to the usefulness of DLVO in describing this
7 complex system. More details on DLVO calculations are provided in the SI.
8
9
10
11
12
13
14
15

16 **3.3 Observations and mechanisms of deposition and detachment on spinach leaf surfaces.**

17
18 Deposition of *E. coli* O157:H7 and *E. coli* 25922 cells was investigated for each strain on
19 its own, and in the presence of each of the two nanoparticles. For combined bacteria-nanoparticle
20 samples, the mixed suspensions were prepared, and aggregation was allowed to occur with the
21 suspension stabilizing for 40 min prior to introduction into the flow cell. The average number of
22 cells observed per experiment across all attachment and detachment scenarios was 177 ± 58 .
23 Presence of nano-CuO in suspension with the cells increased *E. coli* O157:H7 deposition on
24 spinach epicuticle surfaces by nearly 50%, from 14.50 ± 2.39 to $28.11 \pm 2.77 \times 10^{-8}$ m/s, as
25 shown in Figure 2a. There was no significant difference between *E. coli* O157:H7 deposition
26 alone or in the presence of TiO₂ ($16.57 \pm 4.72 \times 10^{-8}$ m/s) ($p > 0.05$). Figure 2b summarizes
27 deposition of *E. coli* 25922 to the epicuticle surface, which was not significantly impacted by the
28 presence of either nanoparticle in suspension during deposition (15.36 ± 1.43 , 12.71 ± 4.29 , and
29 $15.55 \pm 2.32 \times 10^{-8}$ m/s for *E. coli* alone, with CuO, and with TiO₂, respectively) ($p > 0.05$). This
30 may be attributed to its observed high EPS production and agglomeration that screen the impact
31 of nanoparticles on the cell, which is further discussed in Section 3.5.
32
33
34
35
36
37
38
39
40
41
42
43
44
45
46
47
48
49
50

51 Detachment from the epicuticle surface is presented as detachment rate coefficients, in
52 Figures 2a and 2b. Detachment rates of *E. coli* O157:H7 in every scenario were similar, and less
53 than half of the magnitude of the attachment rate coefficients, ranging from -6.05 ± 2.62 to -7.46
54
55
56
57
58
59
60

$\pm 0.89 \times 10^{-8}$ m/s. While no detachment of *E. coli* 25922 was observed over the period of time tested. Additionally, this outcome was not impacted by the presence of either nanoparticle. However, when detachment was normalized by the total cells observed at the end of the attachment phase, nuances in the trends became apparent (Figure 3). Only 5 % of *E. coli* O157:H7 cells in the presence of CuO detached, while 14 % and 18 % of cells were removed when *E. coli* O157:H7 attached alone and in the presence of TiO₂, respectively. The amount of time over which detachment was observed is referred to as “Time to plateau” in Figure 3. This refers to the point in which no additional cells are being removed from the epicuticle surface during the 30 min rinse with DI water. This length of time varied between scenarios, with *E. coli* O157:H7 alone detaching over 13.5 min, O157:H7 with TiO₂ detaching over 14.5 min, and O157:H7 with CuO detaching over just 7.0 min. These results imply that CuO not only increases deposition rates of *E. coli* O157:H7, but also increases the amount of irreversibly attached cells.

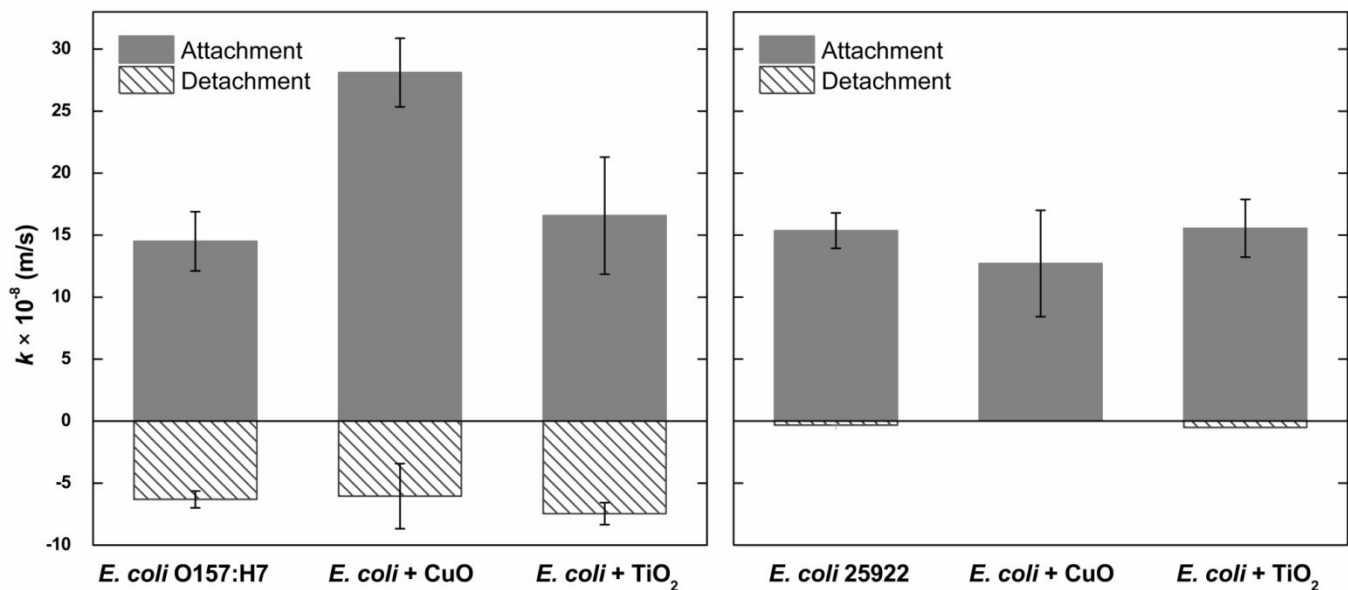


Figure 2. Bacterial deposition and detachment on spinach surface. Attachment (top) and detachment (bottom) mass transfer rate coefficients for *E. coli* O157:H7 (left) and *E. coli* 25922 (right) in 10 mM KCl on spinach leaf surfaces. Error bars represent on standard deviation from 3 replicates.

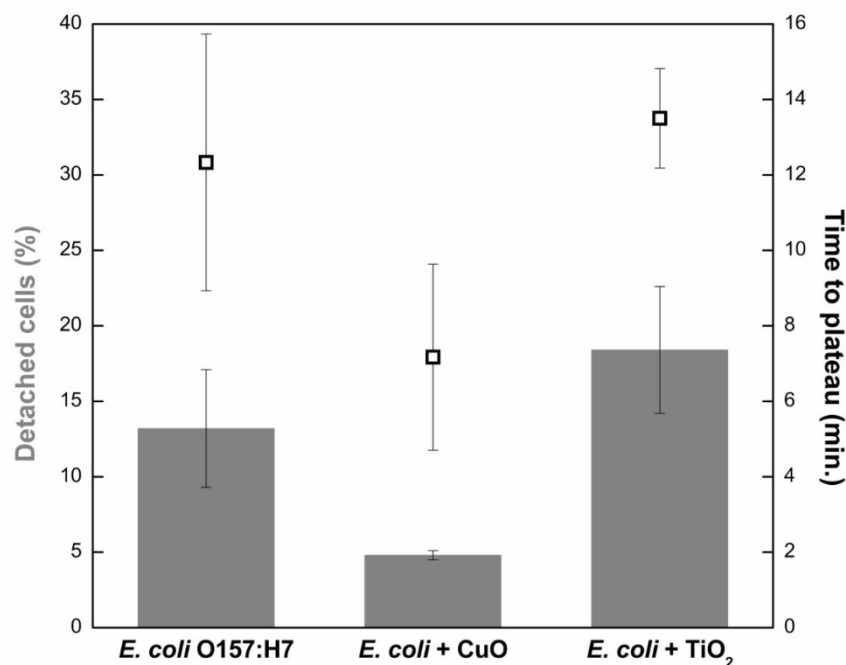


Figure 3. Pathogen detachment from spinach leaf surface. Percentage of *E. coli* O157:H7 cells detached over 30 min with DI water rinse (gray bars, left axis) and time over which the rate of detachment is greater than zero (\square , right axis). Error bars represent the standard deviation calculated from 3 replicates.

3.4 Observations and mechanisms of deposition and release in the packed bed column.

For column experiments, the combined bacteria-nanoparticle suspensions were prepared, and aggregation was allowed to occur and stabilize for 40 min prior to introduction into the column. Breakthrough curves were generated to represent elution of the *E. coli* strains and nanoparticles from the packed bed. Removal of *E. coli* O157:H7 alone and in the presence of nano-CuO was essentially complete ($100.0 \pm 0.4\%$ and $100.0 \pm 0.6\%$, respectively). These scenarios showed minimal release in the phase of the experiment in which the column is flushed (rinsed) with DI H₂O ($1.2 \pm 0.4\%$ and $1.5 \pm 0.6\%$) (Figure 4). Conversely, significantly higher release of $7.5 \pm 2.6\%$ was observed with *E. coli* O157:H7 in the presence of TiO₂ ($p < 0.01$).

In addition to the observed reduction in removal of *E. coli* O157:H7 in the column with TiO₂, breakthrough of TiO₂ particles was also observed in this scenario (Figure 5). This result is

1
2
3 in contrast with control experiments with each nanoparticle alone. In the control experiments,
4 complete removal was observed for both nanoparticles in the simple electrolyte background (data
5 not shown), despite significant repulsive forces between TiO_2 and quartz predicated by particle-
6
7
8
9
10
11
12
13
14
15
16
17
18
19
20
21
22
23
24
25
26
27
28
29
30
31
32
33
34
35
36
37
38
39
40
41
42
43
44
45
46
47
48
49
50
51
52
53
54
55
56
57
58
59
60

in contrast with control experiments with each nanoparticle alone. In the control experiments, complete removal was observed for both nanoparticles in the simple electrolyte background (data not shown), despite significant repulsive forces between TiO_2 and quartz predicated by particle-plate DLVO modeling. It is hypothesized that interactions between *E. coli* O157:H7 cells and TiO_2 in suspension results in increased stability for TiO_2 particles in suspension due to extracellular polymers that have been demonstrated to increase steric hindrance^{30, 60}. Specifically, Chowdhury *et al.* (2012) utilized TiO_2 in a similar column apparatus under similar conditions (pH 7, 10 mg/mL TiO_2 , 10 mM KCl) and also found that particle transport increased in the presence of *E. coli* due to increased electrosteric repulsion³⁰.

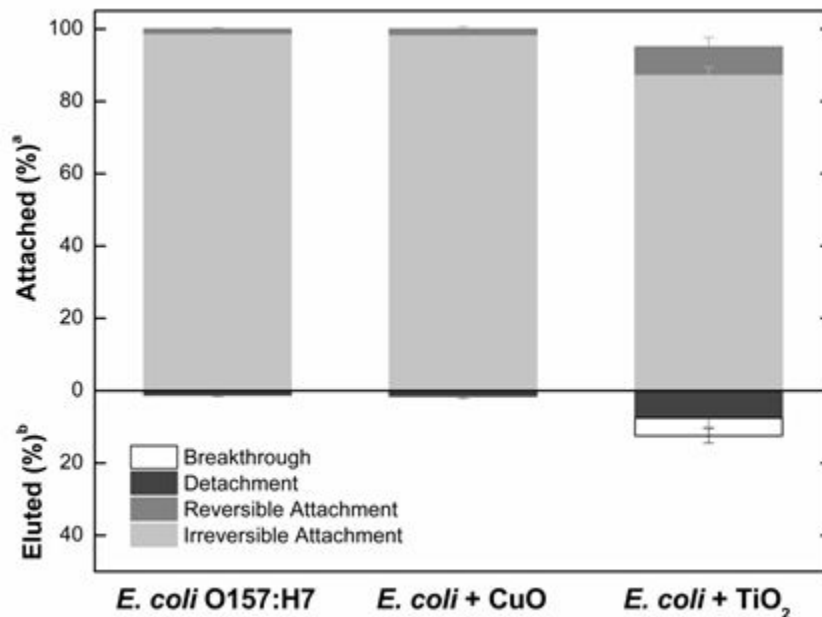


Figure 4. *E. coli* O157:H7 removal and release in the saturated sand column. Breakthrough and release values were calculated by integrating under the breakthrough and DI rinse curves, respectively. Deposition values were calculated using the breakthrough and release values and mass balances. Error bars represent one standard deviation from three replicates.

^a Calculated based on mass balances.

^b Calculated based on UV-VIS absorbance at 600 nm.

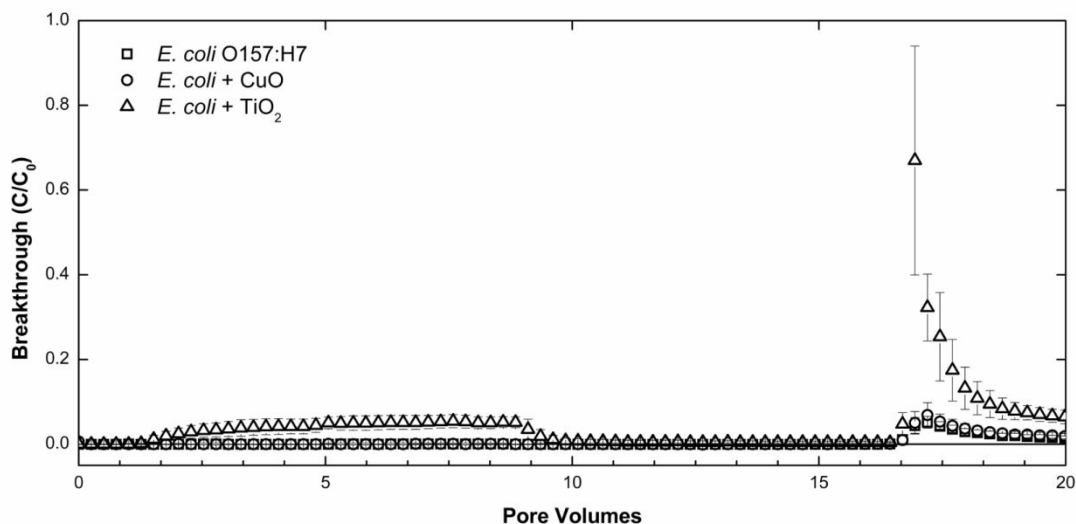


Figure 5. Breakthrough curves for saturated sand column transport experiments with *E. coli* O157:H7. Columns were injected with 10^9 cells/mL in 10 mM KCl electrolyte at pH 7, with or without 10 mg/mL of nanoparticle. Error bars represent one standard deviation from three replicates. Experimental conditions: Darcy velocity = 1 cm/min, Reynolds = 0.1, bed length = 5 cm, bed diameter = 1.5 cm, porosity = 0.45, average grain diameter = $275\mu\text{m}$.

Column retention profiles were created to further elucidate retention trends between these three scenarios (Figure 6). The trends for the suspension of *E. coli* with nanoparticles is based on absorbance values at 600 nm, and is therefore expected to be an indicator of bacterial retention, since cells have higher absorbance than either CuO or TiO₂ particles at the concentrations used in this study (see SI for additional details). The retention curves for the pathogen with nanoparticles show exponential decay in the concentration of retained particles with increasing depth of the column, which is expected based on clean bed filtration theory that is governed by first-order attachment⁵⁵. The shape of the retention curve in for the *E. coli* O157:H7 and TiO₂ suspension suggests that the first 2 cm of the column became saturated with retained particles. In the absence of nanoparticles, nearly linear decay of pathogen retention is observed. This trend is characteristic of zeroth order deposition kinetics, which are not expected for deposition driven by DLVO forces and implies that bacterial retention may be dominated by other mechanisms, such as limited cell surface sorption sites. Based on column porosity, grain size, and relatively high

Darcy velocity (Figure 5), size exclusion is not expected to play a role in the transport and retention of particles in the column. Further discussion of column retention profiles and the potential for physical straining is provided in the Supporting Information.

The presence of nanoparticles appears to increase the retention of suspension species in the porous media. This is suggested by a greater fraction of retention in the upper portion of the column ($C_C/C_N = 0.3, 0.4,$ and 0.5 at the inlet for *E. coli* O157:H7 alone, with TiO_2 , and with CuO , respectively). Specifically, the presence of CuO had a pronounced effect on the retention profile of the *E. coli* O157:H7-nanoparticle suspension. This mirrors the observed increase in bacterial attachment rates to spinach leaf surfaces in the presence of CuO .

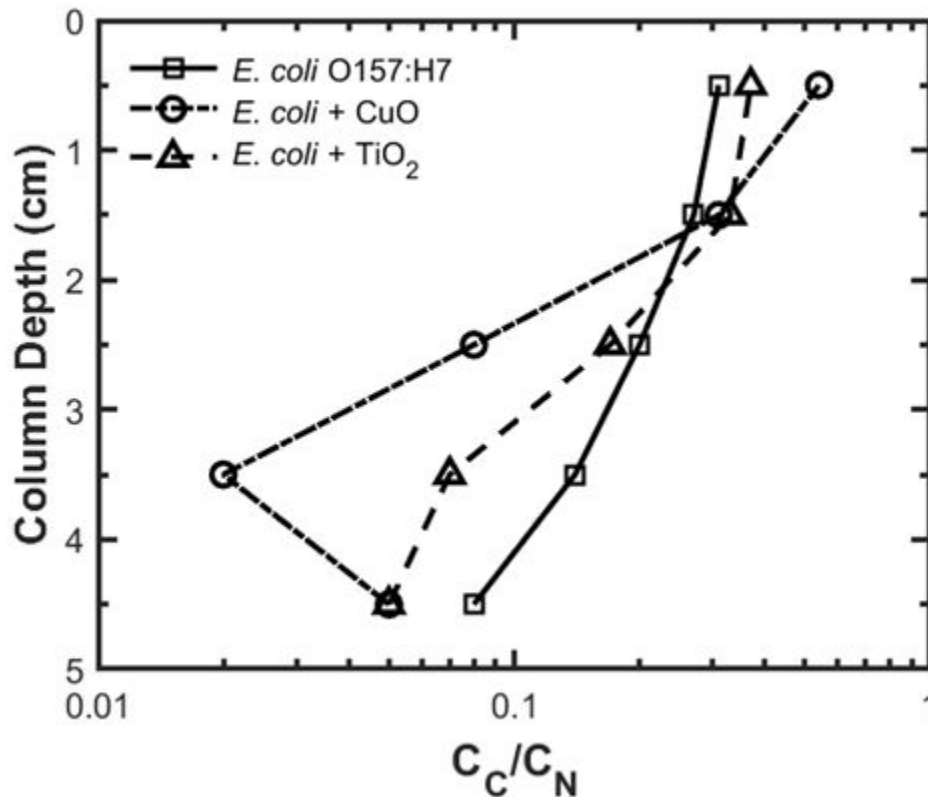


Figure 6. Column retention profiles. Column retention profiles of *E. coli* O157:H7 alone and with each nanoparticle. C_C and C_N are defined as concentration of recovered particles and the sum of concentrations of recovered particles for a given suspension, respectively. A depth of 0 cm corresponds to the entrance of the column.

3.5 Nanoparticle impacts on bacteria fate.

By utilizing and comparing 2D and 3D transport models, the impacts of sub-lethal concentrations of nano-CuO and -TiO₂ on bacterial fate in simplified agricultural environments have been demonstrated. Notably, minimal changes were observed when using *E. coli* 25922 in the presence of nanoparticles. This may be attributed to the highly negative surface charge and greater EPS production of *E. coli* 25922 cells, which is supported by previous studies that have demonstrated enhanced resistance to nanomaterial toxicity by cells that overproduce EPS^{61, 62}. Non-pathogenic *E. coli* 25922 has been utilized in many studies on microbial transport, fate, and influence in agricultural environments as a model microorganism, under the assumption that the results can apply to pathogen fate and thus inform decision-making about associated food safety risks^{41, 63-70}. However, these results make it clear that employing only this non-pathogen surrogate species would drastically underestimate the influence of nanoparticles on bacteria in these environments. In contrast to *E. coli* 25922, the observed changes in fate and transport trends of pathogenic *E. coli* O157:H7 cells were significant and varied by nanoparticle type.

Specifically, nano-CuO caused an increase in irreversible *E. coli* O57:H7 attachment to both leaf and sand surfaces, potentially fostering increased food illness risk by enhancing the early stages of the biofilm formation process. Previous studies have indicated that small amounts of copper-based nanomaterials, on the order of the concentrations employed in this study, can induce stress responses in bacterial cells^{18, 71, 72}. The small primary particle size and near neutral zeta potential may allow nano-CuO particles to interact strongly with the cell surface, or even enter the cell¹⁸. Additionally, CuO can dissolve into copper ions in suspension, which are highly toxic to bacteria^{18, 73}. At these experimental conditions, nano-CuO was demonstrably stable in

1
2
3 solution, as expected based on previous work that found nano-CuO aggregation rates to be
4 correlated with increasing ionic strength⁵². Adeleye *et al.* (2014) found that the presence of
5 bacterial EPS in suspension further increased stability, which lead to increased dissolution of
6 CuO nanoparticles over long term studies in 10 mM NaCl at pH 7 and caused more oxidative
7 stress⁷⁴. One common stress response in bacteria is the overproduction of EPS and increased
8 deposition, in order to begin the process of forming a protective biofilm⁷⁵. Once formed, mature
9 biofilms have been shown to protect *E. coli* O157:H7 cells from several common disinfectants
10 used in the food industry^{76, 77}.

11
12
13
14
15
16
17
18
19
20
21
22 Biofilms also play an important role in microbial fate in soils, which are a central location
23 for the transport and retention of pathogens in the environment. Recent work by Cai *et al.* (2019)
24 demonstrated that different soil minerals can have inhibitory or promotional effects on *E. coli*
25 O157:H7 growth and biofilm formation⁷⁸. Similar to the differential effects of CuO and TiO₂
26 nanoparticles, the impact of soil minerals appeared to be tied to the production of extracellular
27 polymeric substances associated with *E. coli* O157:H7. Observed increases in irreversible
28 pathogen attachment in the presence of nano-CuO indicate that biofilm formation in soils may be
29 enhanced by the deployment of some nanoparticle-based agricultural treatments, presenting a
30 challenge for eliminating pathogens in the field and potentially reducing overall porosity of soils.
31 In contrast, the influence of nano-TiO₂ on bacterial transport in soils was minimal.

32
33
34
35
36
37
38
39
40
41
42
43
44
45
46
47
48
49
50
51
52
53
54
55
56
57
58
59
60
In many ways, nano-TiO₂ is similar to nano-CuO. It has also been demonstrated to have
increasingly stability in the presence of organic matter³⁰ and to induce stress in several types of
bacteria^{79, 80}. However, nano-TiO₂ had no significant impact on the deposition and detachment of
E. coli on the spinach surface, and even reduced irreversible deposition on quartz collectors. This
is similar to work by Jomini *et al.* (2015), which observed an increase in planktonic, versus

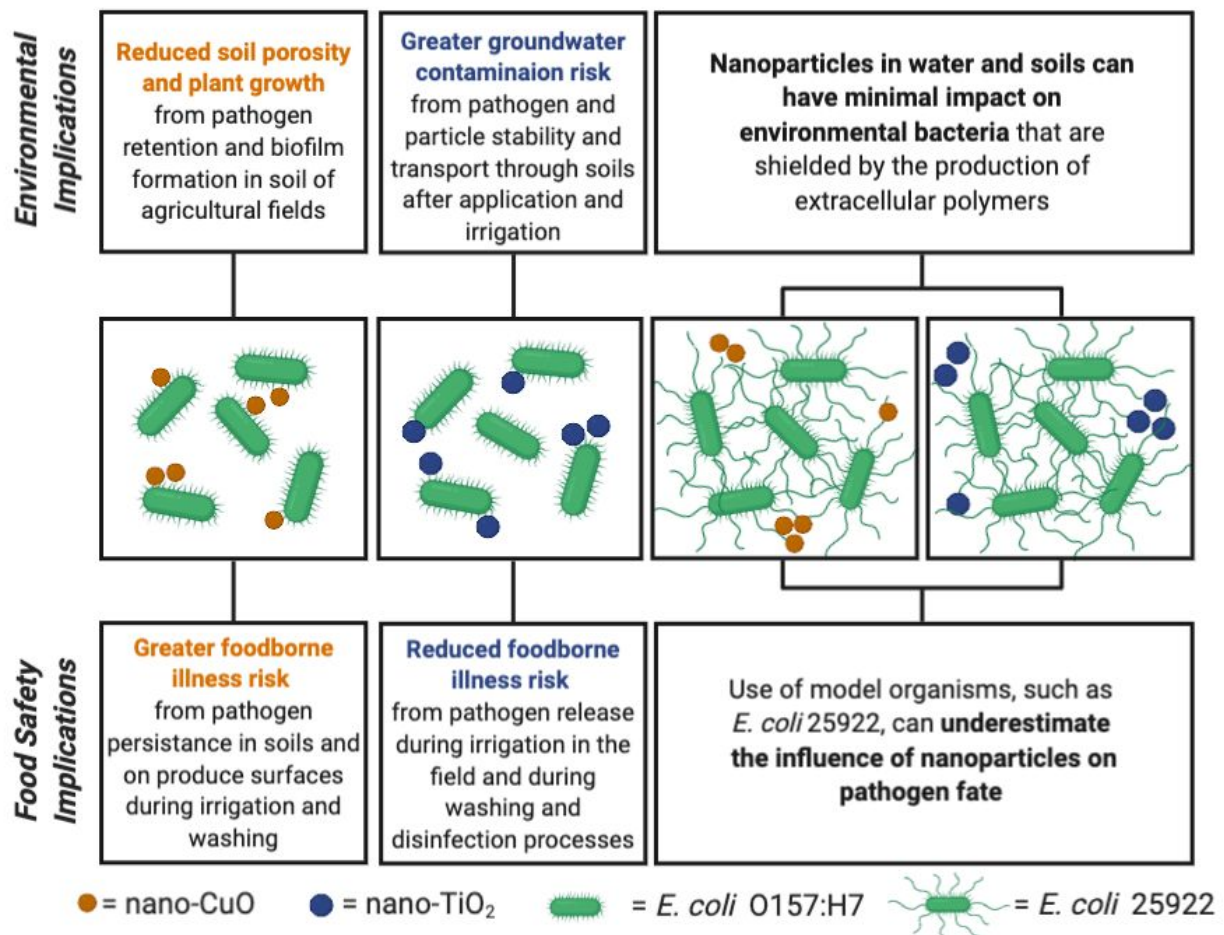
1
2
3 adhered, environmental bacteria over long term exposure to nano-TiO₂⁸¹. One important
4
5 difference between the two studied nanoparticles is that of size: smaller particles tend to be more
6
7 toxic than larger counterparts^{82, 83}, potentially making the antibacterial influence of primary TiO₂
8
9 nanoparticles (~122 nm) less than that of CuO nanoparticles (<50 nm). Further, as evidenced by
10
11 the SEM images in Figure 1, the studied nanoparticles are likely to interact with bacteria cells in
12
13 the form of larger homoaggregates at the tested experimental conditions. Nano-CuO is expected
14
15 to aggregate to approximately 500 nm, while nano-TiO₂ aggregates should be significantly larger
16
17 at approximately 800 nm (Table 1).
18
19
20

21
22 At these solution conditions, TiO₂ is also considerably more negatively charged than
23
24 CuO (-34.5 versus -6.11 mV, respectively). While this does not make it significantly less likely
25
26 to interact with the *E. coli* O157:H7 cells based on DLVO predications, it does result in
27
28 substantial energy barriers between nano-TiO₂ and the spinach and quartz surfaces, which may
29
30 reduce opportunities for particles to interact with adherent bacteria. Further, the antibacterial
31
32 activity of nano-TiO₂ is largely attributed to reactive oxygen species produced through
33
34 photocatalysis. Leung *et al.* (2016) previously observed that light penetration was significantly
35
36 inhibited by bacteria in suspension at 10⁸ cells per mL⁸⁴, resulting in reduced toxicity of TiO₂
37
38 particles that may explain the lesser impact on bacterial transport, in comparison with nano-CuO.
39
40
41

42
43 Low concentrations of nanoparticles have been consistently predicted and monitored in
44
45 environmental waters around the world, on the order of 0.01 – 1 µg/L⁸⁵. However, studies that
46
47 demonstrate the efficacy of these nanoparticles as pesticides and fertilizers have applied
48
49 concentrations between 1 and 1000 mg/L¹⁸⁻²⁵. Therefore, our utilization of 10 mg/L nano-CuO
50
51 and –TiO₂ likely overestimates the influence of nanoparticles in raw environmental waters, but
52
53 may underestimate the effects of direct aqueous applications to leaves and soil in agriculture.
54
55
56
57
58
59
60

Agricultural environments are also likely to have significant amounts of natural organic matter (NOM), unlike the simple systems that were used here. Metal oxide nanoparticles, including nano-CuO and -TiO₂, have been shown to be increasingly stable in the presence of NOM^{30, 54}. This reduction in nanoparticle aggregation could result in greater toxicity and thus more pronounced effects on bacterial cells than observed in this study.

Overall, the results of this work elucidate some impacts of the complex physiochemical interactions between nanoparticles and bacteria by using model systems to simulate aqueous agricultural environments and identify potential food safety risks. Broader implications of these results for environmental and food safety systems are summarized in Figure 7. While



nanoparticles

1
2
3 **Figure 7. Broader implications.** A graphical summary of the broader environmental and food safety implications
4 of these results. Graphic created with BioRender.com.

5 had no significant effects on *E. coli* 25922, nano-CuO (represented by orange in Figure 7)
6
7 increased irreversible attachment rates of *E. coli* O157:H7 cells and nano-TiO₂ (represented by
8 blue in Figure 7) slightly reduced irreversible deposition on quartz surfaces. However, these
9
10 results are based on just two nanoparticle species, as well as one non-pathogen surrogate and one
11
12 foodborne pathogen serovar. It is essential that further research is conducted with additional
13
14 types of nanoparticles, bacteria, and environmental conditions to inform decision-making that
15
16 aims to manage microbial risks throughout the food production and transport system that may
17
18 result from increased use of nanoparticles in agricultural operations.
19
20
21
22
23
24
25
26
27

28 **Conflicts of Interest**

29
30
31 The authors declare that they have no competing financial or non-financial interests.
32
33
34

35 **Acknowledgments**

36
37 This work was supported in part by the National Science Foundation IGERT:
38
39 WaterSENSE - Water Social, Engineering, and Natural Sciences Engagement Program (award
40 number GE-1144635), as well as NSF UC-CEIN award #1266377. The authors thank the staff of
41
42 the Central Facility for Microscopy and Microanalysis at UC Riverside where scanning electron
43
44
45
46
47
48
49
50
51
52
53
54
55
56
57
58
59
60
microscopy was performed.

References

1. Interagency Food Safety Analytics Collaboration. Foodborne illness source attribution estimates for *Salmonella*, *Escherichia coli* O157 (*E. coli* O157), *Listeria monocytogenes* (Lm), and *Campylobacter* using outbreak surveillance data. 2016.
2. World Health Organization (WHO). WHO estimates of the global burden of foodborne diseases: foodborne disease burden epidemiology reference group 2007-2015. 2015.
3. A.N. Olaimat and R.A. Holley, Factors influencing the microbial safety of fresh produce: A review, *Food Microbiology*, 2012, **32**, 1-19.
4. S.A. Bradford and R.W. Harvey, Future research needs involving pathogens in groundwater, *Hydrogeology Journal*, 2017, **25**, 931-938.
5. M. Jongman and L. Korsten, Irrigation water quality and microbial safety of leafy greens in different vegetable production systems: A review, *Food Reviews International*, 2018, **34**, 308-328.
6. Centers for Disease Control and Prevention (CDC). Multistate Outbreak of *E. coli* O157:H7 Infections Linked to Romaine Lettuce (Final Update), 2018 Outbreaks, <https://www.cdc.gov/ecoli/2018/o157h7-04-18/index.html>, (accessed 2018-11-15)
7. N.M. Kinsinger, H.M. Mayton, M.R. Luth, and S.L. Walker, Efficacy of post-harvest rinsing and bleach disinfection of *E. coli* O157: H7 on spinach leaf surfaces, *Food Microbiology*, 2017, **62**, 212-220.
8. Y. Luo, X. Nou, Y. Yang, I. Alegre, E. Turner, H. Feng, M. Abadias, and W. Conway, Determination of free chlorine concentrations needed to prevent *Escherichia coli* O157: H7 cross-contamination during fresh-cut produce wash, *Journal of Food Protection*, 2011, **74**, 352-358.

- 1
2
3 9. C. Goodburn and C.A. Wallace, The microbiological efficacy of decontamination
4 methodologies for fresh produce: a review, *Food Control*, 2013, **32**, 418-427.
5
6
- 7
8 10. A.A. Keller and A. Lazareva, Predicted releases of engineered nanomaterials: From global to
9 regional to local, *Environmental Science & Technology Letters*, 2014, **1**, 65-70.
10
11
- 12 11. M. Kah and T. Hofmann, Nanopesticide research: Current trends and future priorities,
13 *Environment International*, 2014, **63**, 224-235.
14
15
- 16 12. B. Asadishad, S. Chahal, A. Akbari, V. Cianciarelli, M. Azodi, S. Ghoshal, and N. Tufenkji,
17 Amendment of agricultural soil with metal nanoparticles: Effects on soil enzyme activity
18 and microbial community composition, *Environmental Science & Technology*, 2018, **52**,
19 1908-1918.
20
21
22
23
24
25
- 26 13. C.O. Dimkpa and P.S. Bindraban, Nanofertilizers: new products for the industry?, *Journal of*
27 *Agricultural and Food Chemistry*, 2017.
28
29
- 30 14. I. Iavicoli, V. Leso, D.H. Beezhold, and A.A. Shvedova, Nanotechnology in agriculture:
31 Opportunities, toxicological implications, and occupational risks. *Toxicology and applied*
32 *pharmacology*, 2018, **329**, 96–111. doi:10.1016/j.taap.2017.05.025
33
34
35
36
37
- 38 15. I.O. Adisa, V.L. Reddy Pullagurala, J.R. Peralta-Videa, C.O. Dimkpa, W.H. Elmer, J.L.
39 Gardea-Torresdey, and J.C. White, Recent advances in nano-enabled fertilizers and
40 pesticides: a critical review of mechanisms of action. *Environmental Science: Nano*,
41 2019, Advance Article. doi: 10.1039/C9EN00265K
42
43
44
45
46
- 47 16. University of Hertfordshire, Copper (1) Oxide, Pesticide Properties Database (PPDB).
48 <https://sitem.herts.ac.uk/aeru/ppdb/en/Reports/176.htm> (accessed 6-25-2019).
49
50
- 51 17. L. Kiaune and N. Singhasemanon, Pesticidal copper (I) oxide: environmental fate and aquatic
52 toxicity, *Reviews of Environmental Contamination and Toxicology*, 2011, **213**, 1-26.
53
54
55
56
57
58
59
60

- 1
2
3 18. H.A. Ayoub, M. Khairy, S. Elsaid, F.A. Rashwan, and H.F. Abdel-Hafez, Pesticidal Activity
4 of Nanostructured Metal Oxides for Generation of Alternative Pesticide Formulations,
5 *Journal of Agricultural and Food Chemistry*, 2018, **66**, 22, 5491-5498. doi:
6
7 10.1021/acs.jafc.8b01600
8
9
10
11
12 19. Z. Zabrieski, E. Morrell, J. Hortin, C. Dimkpa, J. McLean, D. Britt, A. Anderson, Pesticidal
13 activity of metal oxide nanoparticles on plant pathogenic isolates of *Pythium*,
14 *Ecotoxicology*, 2015, **24**, 1305-1314. doi:10.1007/s10646-015-1505-x
15
16
17
18
19 20. K. Giannousi, I. Avramidis, and C. Dendrinou-Samara, Synthesis, characterization and
20 evaluation of copper based nanoparticles as agrochemicals against *Phytophthora*
21 *infestans*, *RSC Advances*, 2013, **3**, 21743-21752.
22
23
24
25
26 21. F. Yang, C. Liu, F. Gao, M. Su, X. Wu, L. Zheng, F. Hong, and P. Yang, The improvement
27 of spinach growth by nano-anatase TiO₂ treatment is related to nitrogen photoreduction.
28 *Biological Trace Element Research*, 2007, **119**, 77-88.
29
30
31
32
33 22. H. Feizi, P.R. Moghaddam, N. Shahtahmassebi, and A. Fotovat, Impact of bulk and
34 nanosized titanium dioxide (TiO₂) on wheat seed germination and seedling growth.
35 *Biological Trace Element Research*, 2012, **146**, 101-106.23. A. Servin, W. Elmer,
36
37 A. Mukherjee, R. De la Torre-Roche, H. Hamdi, J.C. White, P. Bindraban, and C.
38
39 Dimkpa, A review of the use of engineered nanomaterials to suppress plant disease and
40
41 enhance crop yield, *Journal of Nanoparticle Research*, 2015, **17**, 92.
42
43
44
45
46
47 24. M. Qi, Y. Liu, and T. Li, Nano-TiO₂ Improve the Photosynthesis of Tomato Leaves under
48 Mild Heat Stress, *Biological Trace Element Research*, 2013, **156**, 323-328.
49
50
51
52
53
54
55
56
57
58
59
60

- 1
2
3 25. A. Mattiello and L. Marchiol, Application of Nanotechnology in Agriculture: Assessment of
4
5 TiO₂ Nanoparticle Effects on Barley, Application of Titanium Dioxide, *IntechOpen*, doi:
6
7 10.5772/intechopen.68710
8
9
- 10 26. G. Applerot, J. Lellouche, A. Lipovsky, Y. Nitzan, R. Lubart, A. Gedanken, and E. Banin,
11
12 Understanding the antibacterial mechanism of CuO nanoparticles: Revealing the route of
13
14 induced oxidative stress, *Small*, 2012, **8**, 3326-3337.
15
16
- 17 27. K. Naik and M. Kowshik, Anti-quorum sensing activity of AgCl-TiO₂ nanoparticles with
18
19 potential use as active food packaging material, *Journal of Applied Microbiology*, 2014,
20
21 **117**, 972-983.
22
23
- 24 28. B.R. Singh, B.N. Singh, A. Singh, W. Khan, A.H. Naqvi, and H.B. Singh. Mycofabricated
25
26 biosilver nanoparticles interrupt *Pseudomonas aeruginosa* quorum sensing systems,
27
28 *Scientific Reports*, 2015, **5**, 13719.
29
30
- 31 29. A.A. Keller, A.S. Adeleye, J.R. Conway, K.L. Garner, L. Zhao, G.N. Cherr, J. Hong, J.L.
32
33 Gardea-Torresdey, H.A. Godwin, S. Hanna, Z. Ji, C. Kaweeteerawat, S. Lin, H.S.
34
35 Lenihan, R.J. Miller, A.E. Nel, J.R. Peralta-Videa, S.L. Walker, A.A. Taylor, C. Torres-
36
37 Duarte, J.I. Zink, and N. Zuverza-Mena, Comparative environmental fate and toxicity of
38
39 copper nanomaterials, *NanoImpact*, 2017, **7**, 28-40.
40
41
- 42 30. I. Chowdhury, D.M. Cwiertny, and S.L. Walker, Combined factors influencing the
43
44 aggregation and deposition of nano-TiO₂ in the presence of humic acid and bacteria.
45
46 *Environmental Science & Technology*, 2012, **46**, 6968-6976.
47
48
- 49 31. T.J. Battin, F.V. Kammer, A. Weilhartner, S. Ottofuelling, and T. Hofmann, Nanostructured
50
51 TiO₂: Transport behavior and effects on aquatic microbial communities under
52
53 environmental conditions, *Environmental Science & Technology*, 2009, **43**, 8098-8104.
54
55
56
57
58
59
60

- 1
2
3 32. J.A. Redman, S.L. Walker, and M. Elimelech, Bacterial adhesion and transport in porous
4 media: Role of the secondary energy minimum, *Environmental Science & Technology*,
5 2004, **38**, 1777-1785.
6
7
8
9
10 33. Y. Yang, K. Doudrick, X. Bi, K. Hristovski, P. Herckes, P. Westerhoff, and R. Kaegi,
11 Characterization of food-grade titanium dioxide: the presence of nanosized particles,
12 *Environmental Science & Technology*, 2014, **48**, 6391-6400.
13
14
15
16
17 34. F. Hong, J. Zhou, C. Liu, F. Yang, C. Wu, L. Zheng, and P. Yang, Effect of nano-TiO₂ on
18 photochemical reaction of chloroplasts of spinach, *Biological Trace Element Research*,
19 2005, **105**, 269-279.
20
21
22
23
24 35. M.L. Paret, G.E. Vallad, D.R. Averett, J.B. Jones, and S.M. Olson, Photocatalysis: Effect of
25 light-activated nanoscale formulations of TiO₂ on *Xanthomonas perforans* and control of
26 bacterial spot of tomato, *Phytopathology*, 2013, **103**, 228-236.
27
28
29
30
31 36. I. Chowdhury, Y. Hong, and S.L. Walker, Container to characterization: Impacts of metal
32 oxide handling, preparation, and solution chemistry on particle stability, *Colloids and*
33 *Surfaces A: Physicochemical and Engineering Aspects*, 2010, **368**, 91-95.
34
35
36
37
38 37. L.K. Adams, D.Y. Lyon, P.J.J. Alvarez. Comparative eco-toxicity of nanoscale TiO₂, SiO₂,
39 and ZnO water suspensions, *Water Research*, 2006, **40**, 3527-3532.
40
41
42
43 38. O. Bondarenko, K. Juganson, A. Ivask, K. Kasemets, M. Mortimer, and A. Kahru, Toxicity
44 of Ag, CuO and ZnO nanoparticles to selected environmentally relevant test organisms
45 and mammalian cells in vitro: a critical review, *Archives of Toxicology*, 2013, **87**, 1181-
46
47
48
49
50
51
52
53
54
55
56
57
58
59
60

- 1
2
3 39. T. Waller, I.M. Marcus, and S.L. Walker, Influence of septic system wastewater treatment on
4 titanium dioxide nanoparticle subsurface transport mechanisms. *Analytical and*
5
6 *Bioanalytical Chemistry*, 2018, p. 1-8.
7
8
9
- 10 40. Centers for Disease Control and Prevention (CDC), Reports of Selected E. coli Outbreak
11
12 Investigations: September 20, 2018, <https://www.cdc.gov/ecoli/outbreaks.html>, 2018-11-
13
14 15
15
16
- 17 41. K.L. Cook, E.C. Givan, H.M. Mayton, R.R. Parekh, R. Taylor, and S.L. Walker, Using the
18
19 agricultural environment to select better surrogates for foodborne pathogens associated
20
21 with fresh produce, *International Journal of Food Microbiology*, 2017, **262**, 80-88.
22
23
- 24 42. B. Haznedaroglu, H. Kim, S. Bradford, and S.L. Walker, Relative transport behavior of
25
26 *Escherichia coli* O157: H7 and *Salmonella enterica* serovar *pullorum* in packed bed
27
28 column systems: Influence of solution chemistry and cell concentration, *Environmental*
29
30 *Science & Technology*, 2009, **43**, 1838-1844.
31
32
- 33 43. J.W. McClaine and R.M. Ford, Characterizing the adhesion of motile and nonmotile
34
35 *Escherichia coli* to a glass surface using a parallel-plate flow chamber. *Biotechnology*
36
37 *and Bioengineering*, 2002, **78**, 179-189.
38
39
- 40 44. G. Chen, D.E. Beving, R.S. Bedi, Y.S. Yan, and S.L. Walker, Initial bacterial deposition on
41
42 bare and zeolite-coated aluminum alloy and stainless steel, *Langmuir*, 2009, **25**, 1620-
43
44 1626.
45
46
- 47 45. H.M. Mayton, I.M. Marcus, and S.L. Walker, *Escherichia coli* O157:H7 and *Salmonella*
48
49 *Typhimurium* adhesion to spinach leaf surfaces: Sensitivity to water chemistry and
50
51 nutrient availability, *Food Microbiology*, 2019, **78**, 134-142.
52
53
54
55
56
57
58
59
60

- 1
2
3 46. K. Huang, Y. Tian, D. Salvi, M. Karwe, and N. Nitin, Influence of exposure time, shear
4 stress, and surfactants on detachment of *Escherichia coli* O157:H7 from fresh lettuce leaf
5 surfaces during washing process, *Food Bioprocess Technology*, 2017, **11**, 621-633.
6
7
8
9
10 47. H.N. Kim, S.L. Walker, and S.A. Bradford, Macromolecule mediated transport and retention
11 of *Escherichia coli* O157: H7 in saturated porous media, *Water Research*, 2010, **44**,
12 1082-1093.
13
14
15
16
17 48. Y. Hong, R.J. Honda, N.V. Myung, and S.L. Walker, Transport of iron-based nanoparticles:
18 role of magnetic properties, *Environmental Science & Technology*, 2009, **43**, 8834-8839.
19
20
21 49. J.D. Lanphere, C.J. Luth, and S.L. Walker, Effects of solution chemistry on the transport of
22 graphene oxide in saturated porous media, *Environmental Science & Technology*, 2013,
23 **47**, 4255-4261.
24
25
26
27
28 50. J. Palmer, S. Flint, and J. Brooks, Bacterial cell attachment, the beginning of a biofilm, *J Ind*
29 *Microbiol Biotechnol*, 2007, **34**, 577-588.
30
31
32
33 51. P.M. Stanley, Factors affecting the irreversible attachment of *Pseudomonas aeruginosa* to
34 stainless steel, *Canadian Journal of Microbiology*, 1983, **29**, 1493-1499.
35
36
37
38 52. J.R. Conway, A.S. Adeleye, J.L. Gardea-Torresdey, and A.A. Keller, Aggregation,
39 dissolution, and transformation of copper nanoparticles in natural waters. *Environmental*
40 *Science & Technology*, 2015, **49**, 2749-2756.
41
42
43
44 53. C. Chen, I.M. Marcus, T. Waller, and S.L. Walker, Comparison of filtration mechanisms of
45 food and industrial grade TiO₂ nanoparticles, *Analytical and Bioanalytical Chemistry*,
46 2018, 1-8.
47
48
49
50
51
52
53
54
55
56
57
58
59
60

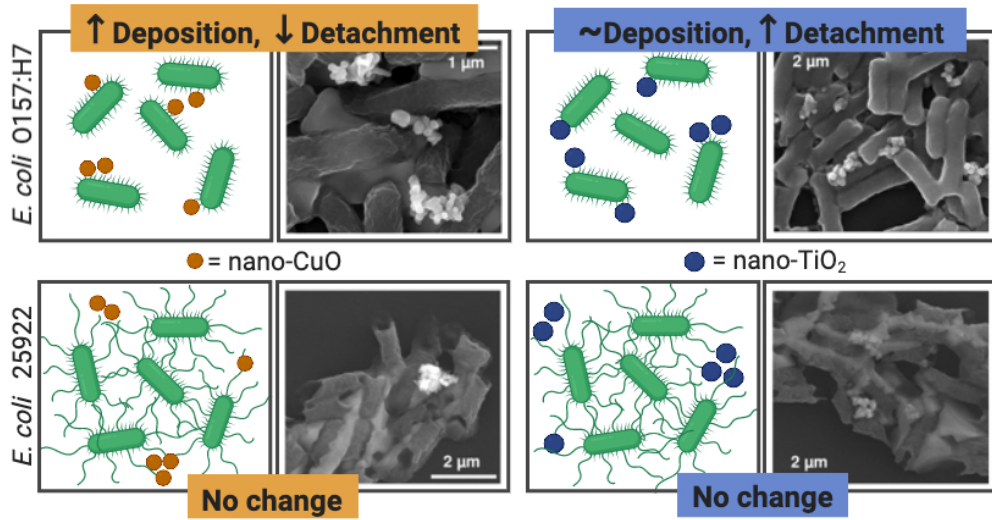
- 1
2
3 54. A.A. Keller, H. Wang, D. Zhou, H.S. Lenihan, G. Cherr, B.J. Cardinale, R. Miller, and Z. Ji,
4
5 Stability and aggregation of metal oxide nanoparticles in natural aqueous matrices,
6
7 *Environmental Science & Technology*, 2010, **44**, 1962-1967.
8
9
- 10 55. S.A. Bradford, J. Simunek, and S.L. Walker, Transport and straining of *E. coli* O157: H7 in
11
12 saturated porous media, *Water Resources Research*, 2006, **42**.
13
14
- 15 56. A. Thill, O. Zeyons, O. Spalla, F. Chauvat, J. Rose, M. Auffan, and A.M. Flank, Cytotoxicity
16
17 of CeO₂ nanoparticles for *Escherichia coli*: Physico-chemical insight of the cytotoxicity
18
19 mechanism, *Environmental Science & Technology*, 2006, **40**, 6151-6156.
20
21
- 22 57. M.J. Hajipour, K.M. Fromm, A.A. Ashkarran, D.J. de Aberasturi, I.R. de Larramendi, T.
23
24 Rojo, V. Serpooshan, W.J. Parak, and M. Mahmoudi, Antibacterial properties of
25
26 nanoparticles, *Trends in Biotechnology*, 2012, **30**, 499-511.
27
28
- 29 58. S.S. Khan, A. Mukherjee, and N. Chandrasekaran, Studies on interaction of colloidal silver
30
31 nanoparticles (SNPs) with five different bacterial species, *Colloids and Surfaces B:*
32
33 *Biointerfaces*, 2011, **87**,129-138.
34
35
- 36 59. B. Derjaguin and L. Landau, Theory of the stability of strongly charged lyophobic sols and of
37
38 the adhesion of strongly charged particles in solutions of electrolytes, *Progress in Surface*
39
40 *Science*, 1993, **43**, 30-59.
41
42
- 43 60. D. Lin, S.D. Story, S.L. Walker, Q. Huang, W. Liang, and P. Cai, Role of pH and ionic
44
45 strength in the aggregation of TiO₂ nanoparticles in the presence of extracellular
46
47 polymeric substances from *Bacillus subtilis*, *Environmental Pollution*, 2017, **228**, 35-42.
48
49
- 50 61. Y. Liu, J. Li, X. Qiu, and C. Burda, Bactericidal activity of nitrogen-doped metal oxide
51
52 nanocatalysts and the influence of bacterial extracellular polymeric substances (EPS),
53
54 *Journal of Photochemistry and Photobiology A: Chemistry*, 2007, **190**, 94-100.
55
56
57
58
59
60

- 1
2
3 62. N. Joshi, B.T. Ngwenya, and C.E. French, Enhanced resistance to nanoparticle toxicity is
4 conferred by overproduction of extracellular polymeric substances, *Journal of Hazardous*
5 *Materials*, 2012, **241**, 363-370.
6
7
8
9
10 63. G. Feng, Y. Cheng, S. Wang, D.A. Borca-Tasciuc, R.W. Worobo, and C.I. Moraru, Bacterial
11 attachment and biofilm formation on surfaces are reduced by small-diameter nanoscale
12 pores: how small is small enough?, *npj Biofilms and Microbiomes*, 2015, **1**, 15022.
13
14
15
16
17 64. L. Gao, J. Hu, X. Zhang, L. Wei, S. Li, Z. Miao, and T. Chai, Application of swine manure
18 on agricultural fields contributes to extended-spectrum β -lactamase-producing
19 *Escherichia coli* spread in Tai'an, China, *Frontiers in Microbiology*, 2015, **6**, 313.
20
21
22
23
24 65. R.S. Suresh Kumar, P.J. Shiny, C.H. Anjali, J.Jerobin, K.M. Goshen, S. Magdassi, A.
25 Mukherjee, and N. Chandrasekaran, Distinctive effects of nano-sized permethrin in the
26 environment, *Environmental Science and Pollution Research*, 2013, **20**, 2593-2602.
27
28
29
30
31 66. N. Talebian, M.R. Nilforoushan, and E.B. Zargar, Enhanced antibacterial performance of
32 hybrid semiconductor nanomaterials: ZnO/SnO₂ nanocomposite thin films, *Applied*
33 *Surface Science*, 2011, **258**, 547-555.
34
35
36
37
38 67. H. Olmez and S.D. Temur, Effects of different sanitizing treatments on biofilms and
39 attachment of *Escherichia coli* and *Listeria monocytogenes* on green leaf lettuce, *LWT -*
40 *Food Science and Technology*, 2010, **43**, 964-970.
41
42
43
44
45 68. W.K. Jung, H.C. Koo, K.W. Kim, S. Shin, S.H. Kim, and Y.H. Park, Antibacterial Activity
46 and Mechanism of Action of the Silver Ion in *Staphylococcus aureus* and *Escherichia*
47 *coli*, *Applied and Environmental Microbiology*, 2008, **74**, 2171-2178.
48
49
50
51
52
53
54
55
56
57
58
59
60

- 1
2
3 69. P. Roslev, L.A. Bjergbaek, and M. Hesselsoe, Effect of oxygen on survival of faecal
4 pollution indicators in drinking water, *Journal of Applied Microbiology*, 2004, **96**, 938-
5 945.
6
7
8
9
10 70. N. Aligiannis, E. Kalpoutzakis, S. Mitaku, and I.B. Chinou, Composition and Antimicrobial
11 Activity of the Essential Oils of Two Origanum Species, *Journal of Agricultural and*
12 *Food Chemistry*, 2001, **49**, 4168-4170.
13
14
15
16
17 71. L.M. Gaetke and C.K. Chow, Copper toxicity, oxidative stress, and antioxidant nutrients,
18 *Toxicology*, 2003, **189**, 147-163.
19
20
21 72. O. Bondarenko, A. Ivask, A. K  inen, and A. Kahru, Sub-toxic effects of CuO nanoparticles
22 on bacteria: Kinetics, role of Cu ions and possible mechanisms of action, *Environmental*
23 *Pollution*, 2012, **169**, 81-89.
24
25
26
27
28 73. Y.W. Baek and Y.J. An, Microbial toxicity of metal oxide nanoparticles (CuO, NiO, ZnO,
29 and Sb₂O₃) to *Escherichia coli*, *Bacillus subtilis*, and *Streptococcus aureus*, *Science of*
30 *the Total Environment*, 2011, **409**, 1603-1608.
31
32
33
34
35 74. A.S. Adeleye, J.R. Conway, T. Perez, P. Rutten, and A.A. Keller, Influence of extracellular
36 polymeric substances on the long-term fate, dissolution, and speciation of copper-based
37 nanoparticles, *Environmental Science & Technology*, 2014, **48**, 12561-12568.
38
39
40
41
42 75. P. Landini, Cross-talk mechanisms in biofilm formation and responses to environmental and
43 physiological stress in *Escherichia coli*, *Research in Microbiology*, 2009, **160**, 259-266.
44
45
46
47 76. B.A. Niemira and P.H. Cooke, *Escherichia coli* O157: H7 biofilm formation on romaine
48 lettuce and spinach leaf surfaces reduces efficacy of irradiation and sodium hypochlorite
49 washes, *Journal of Food Science*, 2010, **75**, 270-277.
50
51
52
53
54
55
56
57
58
59
60

- 1
2
3 77. E.B. Somers, J.L. Schoeni, and A.C. Wong, Effect of trisodium phosphate on biofilm and
4
5 planktonic cells of *Campylobacter jejuni*, *Escherichia coli* O157:H7, *Listeria*
6
7 *monocytogenes* and *Salmonella typhimurium*, *International Journal of Food*
8
9 *Microbiology*, 1994, **22**, 269-276.
- 10
11
12 78. P. Cai, X. Liu, D. Ji, S. Yang, S.L. Walker, Y. Wu, C. Gao, Q. Huang, Impact of soil clay
13
14 minerals on growth, biofilm formation, and virulence gene expression of *Escherichia coli*
15
16 O157:H7, *Environmental Pollution*, 2018, **243**, 953-960.
- 17
18
19 79. A. Kumar, A.K. Pandey, S.S. Singh, R. Shanker, and A. Dhawan, Engineered ZnO and TiO₂
20
21 nanoparticles induce oxidative stress and DNA damage leading to reduced viability of
22
23 *Escherichia coli*, *Free Radical Biology and Medicine*, 2011, **51**, 1872-1881.
- 24
25
26 80. G. Zavilgelsky, V.Y. Kotova, and I. Manukhov, Titanium dioxide (TiO₂) nanoparticles
27
28 induce bacterial stress response detectable by specific lux biosensors, *Nanotechnologies*
29
30 *in Russia*, 2011, **6**, 401-406.
- 31
32
33 81. S. Jomini, H. Clivot, P. Bauda, and C. Pagnout, Impact of manufactured TiO₂ nanoparticles
34
35 on planktonic and sessile bacterial communities, *Environmental Pollution*, 2015, **202**,
36
37 196-204.
- 38
39
40 82. A. Ivask, I. Kurvet, K. Kasemets, I. Blinova, V. Aruoja, S. Suppi, H. Vija, A. Käkinen, T.
41
42 Titma, and M. Heinlaan, Size-dependent toxicity of silver nanoparticles to bacteria, yeast,
43
44 algae, crustaceans and mammalian cells in vitro, *PloS One*, 2014, **9**, e102108.
- 45
46
47 83. S. Nair, A. Sasidharan, V.D. Rani, D. Menon, S. Nair, K. Manzoor, and S. Raina, Role of
48
49 size scale of ZnO nanoparticles and microparticles on toxicity toward bacteria and
50
51 osteoblast cancer cells, *Journal of Materials Science: Materials in Medicine*, 2009, **20**,
52
53 235.
- 54
55
56
57
58
59
60

- 1
2
3 84. Y.H. Leung, X. Xu, A.P.Y. Ma, F. Liu, A.M.C. Ng, Z. Shen, L.A. Gethings, M.Y. Guo, A.B.
4
5 Djurišić, P.K.H. Lee, H.K. Lee, W.K. Chan, and F.C.C. Leung, Toxicity of ZnO and TiO₂
6
7 to *Escherichia coli* cells, *Scientific Reports*, 2016, **6**, DOI: 10.1038/srep35243
8
9
10 85. F. Gottschalk, T.Y. Sun, B. Nowack, Environmental concentrations of engineered
11
12 nanomaterials: Review of modeling and analytical studies, *Environmental Pollution*,
13
14 2013, **181**, 287-300.
15
16
17
18
19
20
21
22
23
24
25
26
27
28
29
30
31
32
33
34
35
36
37
38
39
40
41
42
43
44
45
46
47
48
49
50
51
52
53
54
55
56
57
58
59
60



288x151mm (72 x 72 DPI)

1
2
3
4
5
6
7
8
9
10
11
12
13
14
15
16
17
18
19
20
21
22
23
24
25
26
27
28
29
30
31
32
33
34
35
36
37
38
39
40
41
42
43
44
45
46
47
48
49
50
51
52
53
54
55
56
57
58
59
60